JOURNAL OF AIRCRAFT
Vol. 35, No. 5, September–October 1998

Unsteady Aerodynamic Forces and Aeroelastic Response for External Store of an Aircraft

Deman Tang* and Earl H. Dowell†
Duke University, Durham, North Carolina 27708-0300

An experimental identification investigation of unsteady and stall aerodynamic coefficients for an external store of an aircraft has been made. The coefficient identification is performed by a least-squares procedure based on the measured time series obtained from an aeroelastic model undergoing aerodynamic excitation caused by a gust generator. The results are verified by the good correlation between the theoretical prediction and aerodynamic measurement data. Using the identified unsteady aerodynamic model, numerical investigations for both the stability (flutter) and nonlinear aeroelastic response of this external store model have been made. Also, the results were compared with those obtained from a quasisteady aerodynamic model. It is seen that the effects of unsteady aerodynamics on the nonlinear aeroelastic response are significant when the angle of attack is large.

Nomenclature

a_0 = linear lift curve slope
b_m = linear pitch moment curve slope
C_h, C_ϕ = plunge and pitch moment structural damping coefficients
C_L, C_M = nondimensional lift and pitch moment coefficients, L/qS_0, M_e/lqS_0, respectively
C_{L_1}, C_{M_1} = nondimensional linear lift and pitch moment coefficients
C_{L_2}, C_{M_2} = nondimensional nonlinear lift and pitch moment coefficients
h = dimensional and nondimensional plunge displacement, h/l
J_e = moment of inertia about the elastic axis
K_h = stiffness of store model in plunge deflection
K_ϕ = pitch stiffness of store model about the elastic axis
k = reduced frequency, $\equiv \omega l/2u$
L = lift force
l = length of the store model
M_e = pitch moment about the elastic axis
m = total mass, $m_m + m_s$
m_m = store model mass
m_s = support system mass
q = dynamic pressure, $\frac{1}{2}\rho u^2$
R_0 = maximum cross-sectional radius of the external store model
S_0 = $\equiv \pi R_0^2$
t = time
t_τ = l/u, a reference time
u = flow velocity
u_{cr} = critical flutter velocity
X_m, x_m = distance of the c.g. from the elastic axis, $x_m = X_m/l$
α = angle of attack
α_G = gust angle
Δt = time step
ζ_h, ζ_ϕ = plunge and pitch moment modal damping ratios
θ_0 = initial pitch angle
Λ = eigenvalue matrix
λ_R, λ_I = real and imaginary part of the eigenvalue
ξ = normalized axial distance measured from the tip of model, x/R_0
ρ = air density
ϕ = pitch displacement
ω = frequency
ω_h, ω_ϕ = plunge and pitch moment natural frequencies

Superscripts
$(\cdot)$ = $\mathrm{d}(\ )/\mathrm{d}t$
$\hat{}$ = perturbation variable
$-$ = static equilibrium position

Received Aug. 3, 1997; revision received April 14, 1998; accepted for publication April 15, 1998.

*Research Associate, Department of Mechanical Engineering and Materials Science.
†J. A. Jones Professor and Dean of the School of Engineering.

I. Introduction

LIMIT cycle oscillations (LCOs) have been observed in aeroelastic systems including full-scale aircraft, wind-tunnel models and, of course, in theoretical/numerical models.[1,2] Structural nonlinearities such as freeplay and geometric (strain-displacement) effects have been studied in detail and good correlation between theory (based upon the first principles of mechanics) and experiment has given substantial confidence in our understanding of these effects. In contrast, aerodynamic nonlinearities caused by flow separation still are not describable from theoretical first principles, although a substantial body of experimental data and techniques exists along with useful semiempirical theoretical models.

In the present paper flow separation is modeled using presently available techniques to describe the oscillating flow around a representative external store of an aircraft. Using a semiempirical aerodynamic model, the aeroelastic LCOs are calculated that result from flow separation. The results suggest that flow separation at low Mach numbers alone leads to very large LCOs.

Earlier experimental studies for oscillating two-dimensional airfoils have provided a great deal of important information on the physical mechanisms involved in dynamic stall.[3–13] Usually the airfoil was instrumented with several pressure taps along the airfoil surface. The instantaneous pressure data were then obtained using a set of upper and lower pressure taps and corresponding pressure transducers. The integrated pressure results are normally presented in the body-fixed coordinate system and the resultant integrated loads represented by the pitching moment, C_M, the normal-force coefficient, C_N, and the axial-force coefficient, C_A. The airfoil pitch motion or combined translation/pitch motion is often driven by a mechanical system. This experimental method has been successful for both

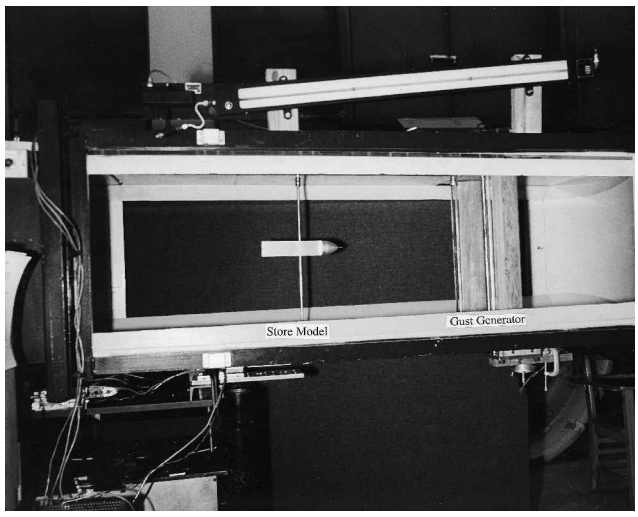

Fig. 1 Photograph of the experimental setup.

two- and three-dimensional airfoils and wings. However, for an external store of the aircraft, a dynamic pressure measurement becomes very difficult because many pressure taps and corresponding transducers would be needed for the complex store structure.

In the present paper a new experimental method is proposed based upon aerodynamic excitation of an aeroelastic system by a gust generator[14] instead of by a mechanical driving system. This gust generator is used to produce a near single harmonic fluid wave in the lateral direction in a wind tunnel, but normal to the model (Fig. 1). The experimental external store model is a simple aeroelastic model with one degree of freedom in plunge or pitch motion. The global lift force or pitch moment acting on the external store is a function of the structural motion as well as the gust field. Thus we can obtain a set of aerodynamic forces from the measured responses (displacement, velocity, and acceleration) for a given gust field. Similar to the ONERA semiempirical theoretical model[11] for dynamic stall aerodynamics, we use the measured aeroelastic response data to identify a system of differential equations relating the aerodynamic forces to the gust field.

Using the identified unsteady aerodynamic model, a comparison between the predictions of a theoretical unsteady and a quasisteady aerodynamic model for the nonlinear aeroelastic response of the store has been made.

II. Experiment Description

All tests of an external bomb carriage model were performed in the Duke University low-speed wind tunnel. The wind tunnel is a closed-circuit tunnel with a test section of 2.3×1.66 ft^2 and a length of 4 ft. For the present test the Reynolds number based upon model length was 0.52×10^6 and the k was varied up to a value of 0.385. The experimental apparatus of the external store model with gust excitation system in the wind tunnel is shown in Fig. 1.

The external store used in this study is a basic carriage model without bombs or rocket-launchers. The geometry of the paraboloidal forebody is described by the following fourth-order polynomial[15]

$$R/R_0 = -0.0436\xi^4 + 0.315\xi^3 - 0.962\xi^2 + 1.507\xi + 0.0028$$

The model is made of an aluminum alloy material. The axial c.g. can be adjusted by adding or subtracting a balance weight from the afterbody of this model. A piece of ground steel bar with a cross section 3/8 in. in diameter and 23 in. in length is passed through the half-length point of the model and welded into this model at the middle of this bar. The ends of the bar are connected to a support system mounted outside of the wind tunnel, at the top and bottom. The support mechanism at each end of the aeroelastic model is a bicantilever beam made of two steel leaf springs that are 203.2 mm long, 28.6 mm wide, and 1.02 mm thick. The distance between the two cantilever beams is 152.4 mm. A support block joins the free ends of the bicantilevered beams on both top and bottom and is free to move in the plunge direction. The two support blocks are the only parts of the support mechanism that move with the model, and this motion is restricted to the plunge degree of freedom. The pitch axis (steel bar) of this external store model is mounted to the upper and lower support blocks through a pair of precision bearings that have a small amount of dry friction in the ball. This design allows the model to have a pitch motion that is independent of the plunge degree of freedom. At the upper bracket there is a spring wire inserted tightly into the pitch axis of the model. The ends of the spring wire are simply supported on the bracket, which provides an adjustable pitch stiffness.

The pitch angle of the model is measured by a rotational velocity/displacement transducer (RVDT), which is fixed at the upper end of the pitch axis. The plunge displacement is measured using another RVDT that measures the motion of the upper support block. A microaccelerometer is mounted on the afterbody of this model that is used to measure the pitch angle acceleration and another accelerometer is mounted on the upper support block to measure the plunge motion acceleration.

The lateral gust velocity u_y (or, hence, α_G, which is equal to u_y/u) was measured with a differential pressure probe mounted on a bar located near the external store model. The bar was attached to a stand fixed on a support table. The pressure probe consisted of two tubes, or claws, oriented at 90 deg to one another in the horizontal plane for measuring the lateral gust. The ends of the tubes protruded from a slender aerodynamic housing, which was oriented in the wind tunnel such that the angle between the tubes was bisected by the freestream. The tubes were connected to a ∓ 0.18-psi differential pressure transducer located outside of the wind tunnel that measured the pressure difference in the lateral direction. For the calibration of this pressure probe, see Ref. 14.

Outputs from these transducers were amplified and sent to an SD 380 signal analyzer and directly recorded on a Macintosh IIci computer through a data-acquisition package, NB-MIO-16, and data-acquisition and analysis software, LabVIEW. To obtain a comparison of the theory with the test, a measurement system calibration was completed before the wind-tunnel test. The dynamic calibration coefficients were determined by a ground vibration test. The following is a complete listing of the system parameters for the experimental model: $R_0 = 0.025$ m, $l = 0.268$ m, $\omega_h = 4.34$ Hz, $\omega_\phi = 6.13$ Hz, $\zeta_h = 0.008$, $\zeta_\phi = 0.021$, $J_e = 0.00844$ kg m^2, m_m (model) $= 0.91$ kg, m_s (supports) $= 1.083$ kg, m (total) $= 1.993$ kg, $K_h = 1480.96$ kg/s^2, and $K_\phi = 12.543$ kg m^2/s^2.

The gust generator consists of an aluminum frame that holds a maximum of two vanes and a motor drive system as shown in Fig. 1. For details of the gust generator, see Ref. 14.

III. Differential Equation Modeling of Unsteady Aerodynamics

A. Perturbed Dynamic Store Equation About a Steady Equilibrium

A two-dimensional linear (typical section) structural model of the bomb carriage is analyzed to investigate linear system stability and nonlinear aeroelastic response resulting from nonlinear (flow separation) aerodynamic forces. Figure 2 shows a sketch of the test setup. The (nonlinear) equations of motion are

$$m\frac{d^2h}{dt^2} - m_m X_m \frac{d^2\phi}{dt^2} + C_h\frac{dh}{dt} + K_h h = -L \qquad (1)$$

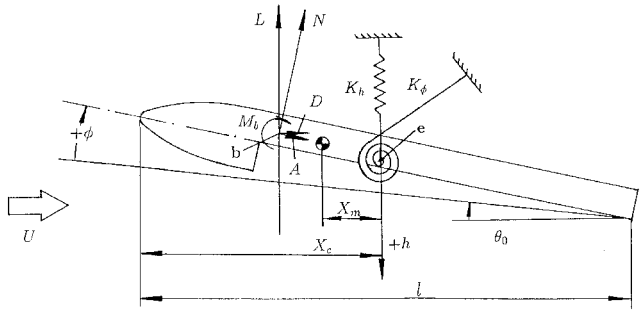

Fig. 2 Sketch of the two-dimensional external store carriage model.

$$J_e \frac{d^2\phi}{dt^2} - m_m X_m \frac{d^2h}{dt^2} + C_\phi \frac{d\phi}{dt} + K_\phi \phi = M_e \tag{2}$$

where X_e is the distance of the elastic axis from the body tip of the model.

Equations (1) and (2) may be written in nondimensional form as

$$\ddot{h} - S_a\ddot{\phi} + 2\zeta_h\omega_h\dot{h} + \omega_h^2 h = -\gamma_L C_L \tag{3}$$

$$\ddot{\phi} - S_h\ddot{h} + 2\zeta_\phi\omega_\phi\dot{\phi} + \omega_\phi^2\phi = \gamma_M C_M \tag{4}$$

where

$$h = h/l, \qquad x_m = X_m/l$$
$$S_a = m_m x_m/m, \qquad S_h = m_m x_m l^2/J_e$$
$$\gamma_L = qS_0/ml, \qquad \gamma_M = qS_0 l/J_e$$

For small-amplitude motion, a perturbation procedure is used.

Let $\phi = \bar{\phi} + \hat{\phi}$, $h = \bar{h} + \hat{h}$, and $\alpha = \bar{\alpha} + \hat{\phi} + (l/u)\dot{\hat{h}} + \alpha_G$, where $\bar{\alpha}$ and $\bar{h}$ are the static equilibrium pitch angle and plunge displacement that are determined using the nonlinear algebraic Eqs. (3) and (4), when $\ddot{h} = \ddot{\phi} = \dot{h} = \dot{\phi} \equiv 0$, $\bar{\phi} = \bar{\alpha} - \theta_0$, and α_G is the gust excitation angle.

Equations (3) and (4) can then be replaced by a set of nonlinear dynamic equations about the static equilibrium position

$$\ddot{\hat{h}} - S_a\ddot{\hat{\phi}} + 2\zeta_h\omega_h\dot{\hat{h}} + \omega_h^2\hat{h} = -\gamma_L C_L(\alpha, \dot{\alpha}) \tag{5}$$

$$\ddot{\hat{\phi}} - S_h\ddot{\hat{h}} + 2\zeta_\phi\omega_\phi\dot{\hat{\phi}} + \omega_\phi^2\hat{\phi} = \gamma_M C_M(\alpha, \dot{\alpha}) \tag{6}$$

Equations (5) and (6) can be used to calculate the aerodynamic coefficients from the measured static and dynamic response data. To improve the accuracy of the measured response data, we consider two cases independently, i.e., in Eq. (5) $\hat{\phi} \equiv 0$ but $\hat{h} \neq 0$, and in Eq. (6) $\hat{h} \equiv 0$ but $\hat{\phi} \neq 0$. Thus we use two independent equations to determine the lift and pitching moment, respectively.

Similar to the two-dimensional ONERA aerodynamic model equations, these lift and pitch moment coefficients can be determined from the following first- and second-order differential equations. For simplicity in expression, we use a subscript z to represent both the lift, C_L, and pitch moment, C_M, and corresponding aerodynamic coefficients

$$C_z = C_{z1} + C_{z2} + s_z t_\tau \dot{\alpha} \tag{7}$$

$$t_\tau \dot{C}_{z1} + \lambda_z C_{z1} = \lambda_z a_0 \alpha + t_\tau \delta_z \dot{\alpha} \tag{8}$$

$$t_\tau^2 \ddot{C}_{z2} + d_z t_\tau \dot{C}_{z2} + \omega_z C_{z2} = -w_z(\Delta C_z + e_z t_\tau \Delta \dot{C}_z) \tag{9}$$

where t_τ and l/u and $\Delta\dot{C}_z = (\partial \Delta C_z/\partial\alpha)\dot{\alpha}$.

The form of Eqs. (7–9) is hypothesized heuristically and has been shown to represent the essential elements of some dynamic stall phenomena.[11]

In this paper quasisteady aerodynamics means that the relationship between C_L and α is simply the static one, whereas unsteady means that the relationship between C_L and α is given by Eqs. (7–9). Note, however, that both models use Eqs. (5) and (6), which itself invokes a quasisteady relationship among α, ϕ, and $\dot{h}$. To make the ONERA model truly unsteady, it would be necessary to separately and distinctly account for the effects of ϕ (and $\dot{\phi}$) on the one hand and $\dot{h}$ on the other. We note that some authors, e.g., Tobak,[16] have made this distinction in their models.

B. Determination of Static Aerodynamics

Using Eqs. (5) and (6), we measure the static plunge displacement and pitch angle to determine the static lift and pitch moment for several initial pitch angles, θ_0, when the perturbation responses are zero (there is no gust excitation). The static lift and pitch moment coefficients are nonlinear for the whole measurement range of the initial pitch angle $\theta_0 = -25$ to 25 deg (see Fig. 3 for an airspeed of $u = 25.7$ m/s). In Fig. 3 the symbol ◇ denotes the experimental data and the solid line the results from a curve fitting method. Similar results for C_M are also obtained. Note that the experimental data are time-averaged values. Because of turbulent wake vortices, there are slight fluctuations about the static value that increase with the initial pitch angle even when there is no gust excitation.

From the quasistatic aerodynamic coefficients, we choose a reference condition, say, $\alpha = 0$.

Let $a_0 = (dC_{z0}/d\alpha)|_{\alpha=0}$.

Then the static lift (or pitch moment) coefficient C_{z0} is defined to have two domains: the linear part, $C_{z0} = a_0\alpha$ and the nonlinear part, $C_{z0} = a_0\alpha + \Delta C_z$, where ΔC_z is the difference

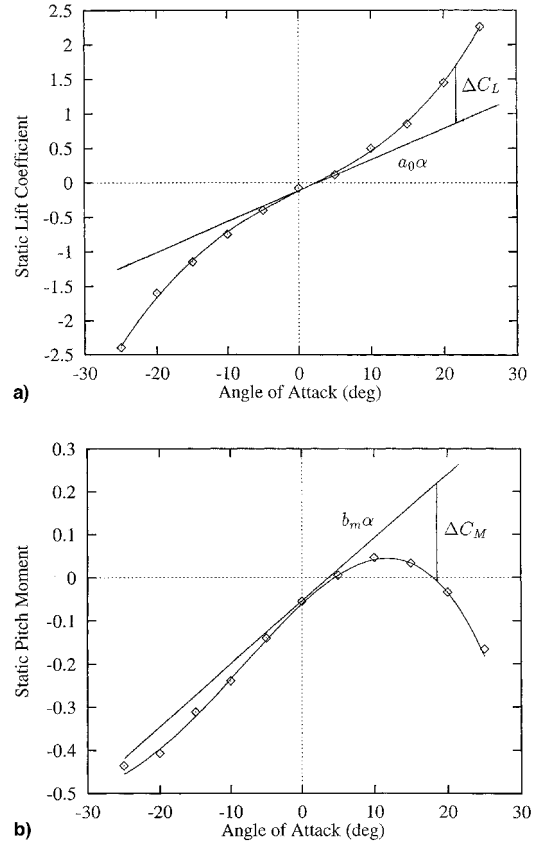

Fig. 3 Experimental and curve-fitting static aerodynamic coefficients vs α. ◇ from the experimental data and —— from curve-fitting method: a) lift (C_L) and b) pitch moment about mid-length (C_M).

between the linear characteristic extended up to the maximum incidence and the true lift (or pitch moment) coefficient C_{z0}

$$\Delta C_z = \begin{cases} 0 & \text{if} \quad \alpha \le \alpha_s \\ a_0\alpha - C_{z0} & \text{otherwise} \end{cases} \tag{10}$$

C. Identification of Unsteady Aerodynamic Coefficients

Equations (5–9) represent the coupling of the unsteady aerodynamics with the structural response. For determination of the aerodynamic coefficients, an identification technique in the time domain and a least-squares procedure (LSP) is proposed. The method is described in the following text.

Consider a measured time history, $x(t)$, with a constant sampling time step length, Δt. The sampled version of $x(t)$ is then defined by

$$x(i) = x[(i - 1)\Delta t] \qquad i = 1, 2, \ldots, N$$

The total time T is given by

$$T = (N - 1)\Delta t$$

The velocity and acceleration of this time series can be derived by three-point formulas:

$$\dot{x}(i) = (1/2\Delta t)[x(i + 1) - x(i - 1)]$$

$$\ddot{x}(i) = [1/(\Delta t)^2][x(i - 1) - 2x(i) + x(i + 1)]$$

From Eqs. (5) and (6) we can obtain the time-series data of the lift and the pitch moment coefficients $C_L(i)$ and $C_M(i)$ for a given airspeed, u, and initial pitch angle, θ_0. Note that to improve accuracy we directly use the measured acceleration signal that is passed through a low-pass filter and the velocity is obtained using a three-point formula in our experiment.

The identification procedure includes two steps.

Step 1, determination of the linear differential equation coefficients: Set the experimental model to have a zero initial pitch angle and the airspeed at some fixed value, say, $u = 25.7$ m/s. The gust excitation frequency is set very close or equal to the plunge (or pitch) natural frequency. Then we measure the plunge (or pitch) displacement and acceleration signals of this model and the gust lateral velocity. From Eq. (8), one has

$$C_{z1}(i + 1) = \frac{t_\tau\delta_z/2\Delta t + \lambda_z a_0/2}{t_\tau/2\Delta t + \lambda_z/2}\,\alpha(i + 1)$$

$$C_{z1}(i - 1) = \frac{-t_\tau\delta_z/2\Delta t + \lambda_z a_0/2}{-t_\tau/2\Delta t + \lambda_z/2}\,\alpha(i - 1)$$

$$C_z(i + 1) = C_{z1}(i + 1) + \frac{t_\tau s_z}{2\Delta t}\,\alpha(i + 1)$$

$$C_z(i - 1) = C_{z1}(i - 1) - \frac{t_\tau s_z}{2\Delta t}\,\alpha(i - 1)$$

Let

$$q_1 = \frac{\delta_z}{1 + \Delta t\lambda_z/t_\tau}, \qquad q_2 = \frac{\lambda_z}{1 + \Delta t\lambda_z/t_\tau}, \qquad q_3 = s_z$$

Then at $(i + 1)$th point in time, we have

$$C_z(i + 1) = \left[\alpha(i + 1), \quad \frac{a_0\Delta t\alpha(i + 1)}{t_\tau}, \quad \frac{t_\tau\alpha(i + 1)}{2\Delta t}\right]\{q_1, q_2, q_3\}^T \tag{11}$$

If we assume the gust excitation frequency is ω and $T = 2\pi/\omega$, then in a period we have N measurement points in time. The response may be formulated in matrix form for each individual time step of $j = 3 \times i (i = 1, 2, \ldots, N/3)$.

$$\{Z_1\}_{N/3\times 1} = [Y_1]_{N/3\times 3}\{Q_1\}_{3\times 1} \tag{12}$$

If $\{Z_1\}$ is from the measured lift or pitch moment coefficient, $C_L(i + 1)$, $C_M(i + 1)$, respectively, the optimized coefficients in $\{Q_1\}$ may be determined such that residual sum of squares of $\{S_1\}$ becomes a minimum for all time points

$$\{S_1\} = \{Z_1\}_{N/3\times 1} - [Y_1]_{N/3\times 3}\{Q_1\}_{3\times 1} \tag{13}$$

The condition of minimum error leads to

$$|\{S_1\}^T\{S_1\}| \Rightarrow \min, \qquad \{Q_1\} = ([Y_1]^T[Y_1])^{-1}[Y_1]^T\{Z_1\} \tag{14}$$

The linear unsteady aerodynamic coefficients, λ_z, δ_z, and s_z can be solved from the known matrix $\{Q_1\}$; they are $\lambda_z = q_2/(1 - \Delta t q_2/t_\tau)$, $\delta_z = q_1(1 + \Delta t\lambda_z/t_\tau)$, and $s_z = q_3$.

Step 2, determination of the nonlinear differential equation coefficients: Similar to the procedure in the linear part, the state equations at each time step are obtained from Eq. (9):

$$C_{z2}(i + 1) = \frac{-w_z[(\Delta t)^2 + \Delta t e_z t_\tau]}{2t_\tau^2 + d_z t_\tau\Delta t + (\Delta t)^2 w_z}\,\Delta C_z(i + 1)$$

$$C_{z2}(i - 1) = \frac{-w_z[(\Delta t)^2 - \Delta t e_z t_\tau]}{2t_\tau^2 - d_z t_\tau\Delta t + (\Delta t)^2 w_z}\,\Delta C_z(i - 1)$$

Let

$$p_1 = \frac{w_z}{2t_\tau^2 + d_z t_\tau\Delta t + (\Delta t)^2 w_z}, \qquad p_2 = \frac{w_z e_z}{2t_\tau^2 + d_z t_\tau\Delta t + (\Delta t)^2 w_z}$$

$$p_3 = \frac{w_z}{2t_\tau^2 - d_z t_\tau\Delta t + (\Delta t)^2 w_z}, \qquad p_4 = \frac{w_z e_z}{2t_\tau^2 - d_z t_\tau\Delta t + (\Delta t)^2 w_z}$$

Then at $(i + 1)$th and $(i - 1)$th points in time, we have

$$C_{z2}(i + 1) = [-(\Delta t)^2\Delta C_z(i + 1), -t_\tau\Delta t\Delta C_z(i + 1)]\{p_1, p_2\}^T \tag{15}$$

$$C_{z2}(i - 1) = [-(\Delta t)^2\Delta C_z(i - 1), t_\tau\Delta t\Delta C_z(i - 1)]\{p_3, p_4\}^T \tag{16}$$

The matrix equation for each individual time step is

$$\{Z_2\}_{2N/3\times 1} = [Y_2]_{2N/3\times 4}\{Q_2\}_{4\times 1} \tag{17}$$

where $\{Q_2\} = \{p_1, p_2, p_3, p_4\}$ and $\{Z_2\}$ is the difference between the measured lift or pitch moment coefficient time history $C_L(i + 1)$, $C_L(i - 1)$, $C_M(i + 1)$, $C_M(i - 1)$ and the linear components. They are

$$Z_2(i + 1) = C_z(i + 1) - C_{z1}(i + 1) - s_z t_\tau\alpha(i + 1)/2\Delta t$$

$$Z_2(i - 1) = C_z(i - 1) - C_{z1}(i - 1) + s_z t_\tau\alpha(i - 1)/2\Delta t$$

Using the condition of minimum error, we have

$$\{Q_2\} = ([Y_2]^T[Y_2])^{-1}[Y_2]^T\{Z_2\} \tag{18}$$

The nonlinear unsteady aerodynamic coefficients, w_z, d_z, and e_z can be determined from the known matrix $\{Q_2\}$; they are

$$e_z = p_2/p_1$$

$$2t_\tau^2(1 - p_1/p_3) - d_z t_\tau\Delta t(1 + p_1/p_3) + (\Delta t)^2(1 - p_1/p_3)w_z = 0$$

$$2t_\tau^2 p_1 - d_z t_\tau\Delta t p_1 + [(\Delta t)^2 p_1 - 1]w_z = 0$$

D. Experimental Results for Unsteady Aerodynamic Coefficients

The experimental results for the unsteady lift and pitch moment coefficients about the mid-length are described as follows. The airspeed was kept constant at 25.7 ± 0.5 m/s. The θ_0 was varied between −25 and 25 deg. The sample rate is Δt = 1/800 and the total sample number is N = 800.

1. *Unsteady Lift Aerodynamic Coefficients*

In this case the gust excitation frequency was kept constant at ω = 4.29 Hz (note that ω_h = 4.34 Hz). First we identify the linear unsteady aerodynamic coefficients using zero initial pitch angle. It is found from the static test that when θ_0 = 0 deg, the angle of attack at the static equilibrium state is 0 deg. Therefore, θ_0 = 0 deg is taken as the reference condition and the corresponding lift curve slope at this angle of attack is a_0 = 2.99.

Figures 4a and 4b show the measured time-history signals of the plunge displacement, h, angle of attack, α, for θ_0 = 0 deg. The angle of attack is dominated by the gust part and the contribution of the plunge motion to α is smaller by comparison. The gust-angle amplitude is itself small, near 1 deg (thus the linear assumption is reasonable in this small excitation range). The gust field is not a pure single harmonic wave. A 2ω gust component is also observable. Because the excitation frequency is very close to the plunge natural frequency, the displacement response and the lift coefficient nevertheless are almost single harmonic. However, because the gust is not a very steady single harmonic wave, an averaging procedure is made in the identification. We take four cycles of sample data from the total measured signals, and then use each cycle data to identify a set of linear and nonlinear aerodynamic coefficients using Eq. (14). The average values are listed as follows: λ_L = 0.195, δ_L = 1.615, and s_L = 2.51.

From the measured time histories of lift coefficient and angle of attack, we can obtain the lift hysteresis loop plot as shown in the dashed line of Fig. 4c for a 1-s time history. For comparison, the theoretical results using the identified parameters are also plotted in this figure as shown by the solid line. The agreement is reasonably good.

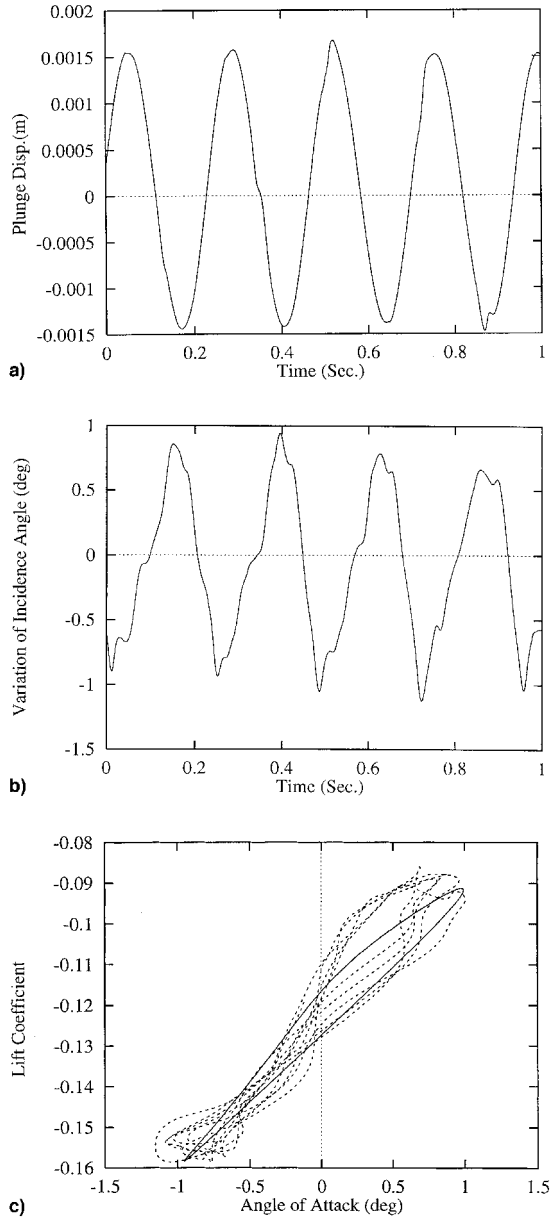

Fig. 4 Time histories of the plunge motion and lift hysteresis loop for θ_0 = 0 deg and airspeed u = 25.7 m/s: a) plunge displacement h, b) variation of α, and c) lift hysteresis loop plot.

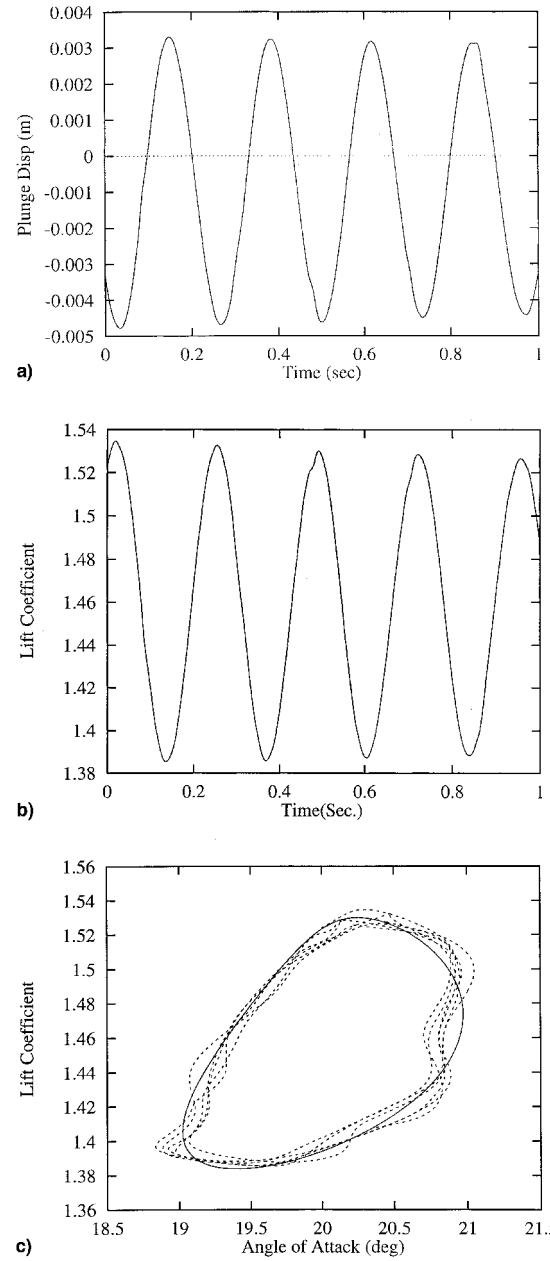

Fig. 5 Time histories of the plunge motion, lift coefficient, and lift hysteresis loop for θ_0 = 20 deg and airspeed u = 25.7 m/s: a) plunge displacement h, b) lift coefficient C_L, and c) lift hysteresis loop plot.

Figures 5a and 5b show the typical measured time-history signals of the plunge displacement, h, and the lift coefficient, C_L, for $\theta_0 = 20$ deg. As compared with Fig. 4, the plunge response amplitude and lift coefficient are significantly increased. Figure 5c shows the comparison between the experimental and theoretical results for the lift hysteresis loop. The symbols are the same as shown in Fig. 4. The aerodynamic hysteresis damping increases as the initial pitch angle increases. The results are similar to the results for a two-dimensional airfoil.[10]

Using Eq. (18) and various initial pitch angles, we obtain a set of averaged nonlinear aerodynamic coefficients. The results are shown by the ◇ symbol (test) and solid line (curve fitting) in Fig. 6 for the nonlinear aerodynamic coefficients, w_L, d_L, and e_L vs the static equilibrium α. These coefficients will be applied to a nonlinear aeroelastic analysis of this model in Sec. IV.

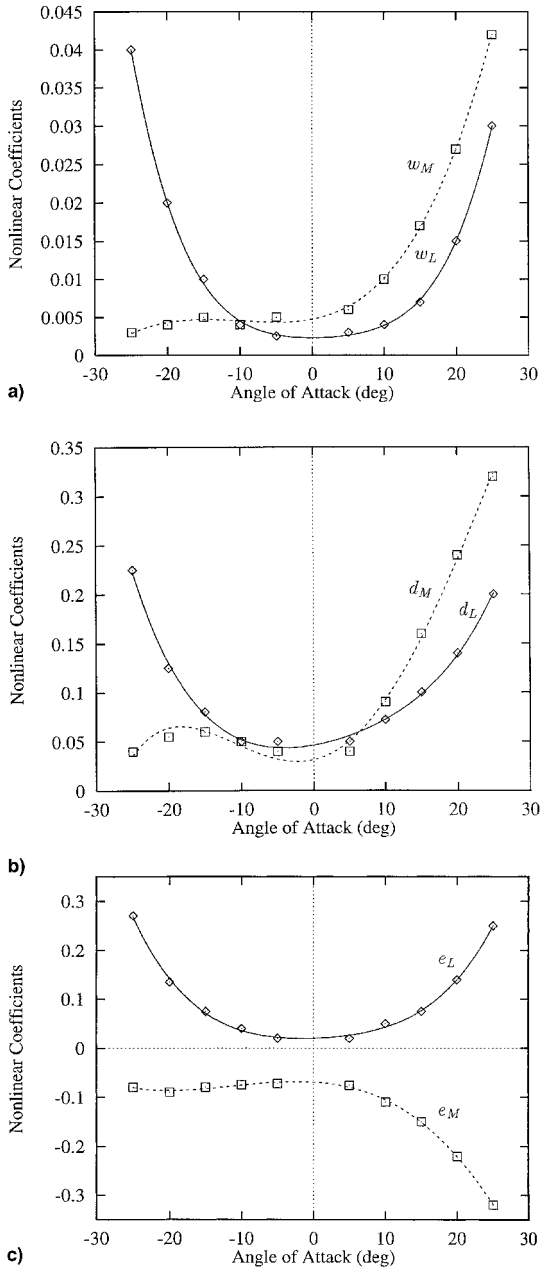

Fig. 6 Identified nonlinear aerodynamic coefficients vs α. ◇ and □ are from the experimental data, and ——, lift, and ---, pitch moment lines are from curve-fitting method: a) w_L, w_M b) d_L, d_M and c) e_L, e_M

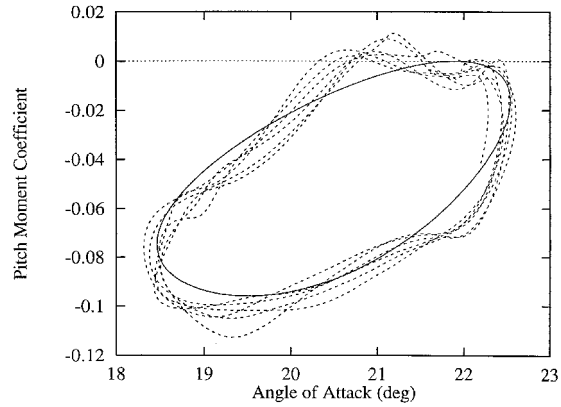

Fig. 7 Pitch moment hysteresis loop plot for $\theta_0 = 20$ deg and airspeed $u = 25.7$ m/s.

2. Unsteady Pitch Moment Aerodynamic Coefficients

The gust excitation frequency was kept constant at $\omega = 6.2$ Hz (note that $\omega_\phi = 6.13$ Hz) for all initial pitch angles. First, we identify the linear unsteady aerodynamic coefficients using a small initial pitch angle. From the static test we found the zero initial pitch angle corresponds to a static equilibrium angle of attack of 0.072 deg, which is very close to the zero initial pitch angle. We take this point as a reference condition and the corresponding pitch moment curve slope at this angle of attack is $b_m = 0.88$. We take six cycles of sample data from the total measured signals, and then use each cycle data to identify a set of linear and nonlinear aerodynamic coefficients.

A set of averaged linear aerodynamic coefficients is determined as follows: $\lambda_M = 0.32$, $\delta_M = -3.1$, and $s_M = 1.2$. And nonlinear aerodynamic coefficients, w_M, d_M, and e_M vs the static equilibrium α are shown by the □ symbol (test) and the broken line (curve fitting) in Fig. 6.

Figure 7 shows the typical experimental and theoretical result for the pitch moment hysteresis loop for $\theta_0 = 20$ deg. The symbols are the same as shown in Fig. 5c. The aerodynamic hysteresis pitch damping increases with the initial pitch angle. The agreement between the theory and experiment is good.

IV. Nonlinear Aeroelastic Analysis

Nonlinear aeroelastic analysis of this external store model includes stability (flutter) of the linearized equations and a nonlinear aeroelastic response (LCO) without gust excitation. The model parameters were earlier in this paper. The plunge and pitch natural frequencies are now $\omega_h = 1.5$ Hz and $\omega_\phi = 2.0$ Hz.

A. Stability Analysis (Flutter)

For a stability analysis of the external store model with nonlinear unsteady aerodynamics, a perturbation approach is used. The linearized dynamic perturbation equations of the external store system about a static equilibrium state are

$$\ddot{\hat{h}} - S_\alpha \ddot{\hat{\phi}} + 2\zeta_h \omega_h \dot{\hat{h}} + \omega_h^2 \hat{h} + \gamma_L \hat{C}_L = 0 \tag{19}$$

$$\ddot{\hat{\phi}} - S_h \ddot{\hat{h}} + 2\zeta_\phi \omega_\phi \dot{\hat{\phi}} + \omega_\phi^2 \hat{\phi} - \gamma_M \hat{C}_M = 0 \tag{20}$$

and the linearized dynamic perturbation equations of the aerodynamic model are

$$\hat{C}_l = \hat{C}_{z1} + \hat{C}_{z2} + s_z t_\tau \dot{\hat{\alpha}} \tag{21}$$

$$t_\tau \dot{\hat{C}}_{z1} + \lambda_z \hat{C}_{z1} = \lambda_z a_0 \hat{\alpha} + t_\tau \delta_z \dot{\hat{\alpha}} \tag{22}$$

$$t_\tau^2 \ddot{\hat{C}}_{z2} + d_z t_\tau \dot{\hat{C}}_{z2} + w_z \hat{C}_{z2} = -w_z \frac{\partial \Delta C_z}{\partial \alpha} \hat{\alpha} - w_z e_z t_\tau \frac{\partial \Delta C_z}{\partial \alpha} \dot{\hat{\alpha}} \tag{23}$$

These equations can be put into state-variable form yielding

$$\{\dot{\chi}\} + [\mathcal{A}]\{\chi\} = \{\mathcal{O}\} \tag{24}$$

where the variable matrix $\{\chi\}$ is expressed as a set of structural motion and aerodynamic coefficient variables, $\{\chi\} = \{\hat{h}, \dot{\hat{h}}, \hat{\phi}, \dot{\hat{\phi}}, \hat{C}_{L_1}, \hat{C}_{L_2}, \dot{\hat{C}}_{L_2}, \hat{C}_{M_1}, \hat{C}_{M_2}, \dot{\hat{C}}_{M_2}\}$.

The flutter critical speed is determined by solving the preceding eigenvalue problem. The solution depends on θ_0. Thus, we form $\hat{h} = \bar{h}e^{\lambda\tau}$, $\hat{\phi} = \bar{\phi}e^{\lambda\tau}$, $\hat{C}_{L_1} = \bar{C}_{L_1}e^{\lambda\tau}$, $\hat{C}_{L_2} = \bar{C}_{L_2}e^{\lambda\tau}$, $\hat{C}_{M_1} = \bar{C}_{M_1}e^{\lambda\tau}$, and $\hat{C}_{M_2} = \bar{C}_{M_2}e^{\lambda\tau}$, and determine the eigenvalues λ in the usual way.

B. Nonlinear Aeroelastic Response

To determine the nonlinear aeroelastic response in the time domain, a similar perturbation procedure is used.

Let

$$\phi = \bar{\phi} + \hat{\phi}, \qquad h = \bar{h} + \hat{h}, \qquad \alpha = \bar{\alpha} + \hat{\phi} + (l/u)\dot{\hat{h}} \tag{25}$$

where $\bar{\alpha}$ and $\bar{h}$ are the static equilibrium pitch angle and plunge displacement determined using the nonlinear algebraic Eqs. (3) and (4), when $\dot{h} = \ddot{\phi} = \dot{h} = \phi \equiv 0$, and $\bar{\phi} = \bar{\alpha} - \theta_0$.

We use Eqs. (5) and (9) to calculate the transient response. The direct numerical time integration uses a standard computational code. The integral step length is $\Delta t = 1/100$ s.

V. Numerical Investigation Results

A. Stability Analysis (Flutter)

Figure 8 shows typical eigenvalue solutions of the linearized system [Eq. (24)] for $\theta_0 = -5$ deg and $x_m = -0.06$. Figure 8a presents the real part of the eigenvalue, λ, vs the flow velocity. We find there are two intersections with the velocity axis. One is for $u_f = 28.5$ m/s, and another is for $u_A = 58.5$ m/s; u_f is the critical flutter velocity with a corresponding flutter oscillatory frequency, $\omega_f = 9.8$ rad/s, and u_A is called a higher-order flutter velocity with a corresponding oscillatory frequency, $\omega_A = 8.4$ rad/s. Figure 8c is a root-locus plot that indicates that the flutter is dominated by the plunge motion for the first critical velocity and by the pitch motion for the second critical velocity. Results from a simpler quasisteady aerodynamic model (Figs. 8b and 8d), are also plotted. The critical flutter velocity is now 30.75 m/s, which is dominated by the plunge motion.

Figure 9 shows the flutter velocity vs the initial pitch angle θ_0 for $x_m = -0.66$. The □ symbol indicates the results from the quasisteady aerodynamics, and the ◇ and △ symbols indicate the results from unsteady aerodynamics. The results show good agreement in the range of $\theta_0 = -5$ to 2.5 deg. Beyond this range there is a large quantitative difference, particularly at the larger initial pitch angles. One may conclude that the effect of unsteady aerodynamics on the flutter instability is significant for the larger angles of attack.

B. Nonlinear Aeroelastic Response

Results for the quasisteady case: Figure 10a shows the limit cycle pitch amplitude (peak) vs flow velocity for an initial angle of $\theta_0 = -5$ deg. At $u = 30.51$ m/s (recall that $u = 30.5$ m/s is the critical flutter velocity of the linearized system), the pitch amplitude of limit cycle oscillation (LCO) is $\hat{\phi} = 2.75$ deg. The pitch amplitude of LCO increases with the flow velocity. A typical time history of LCO for $u = 30.52$ is shown in Fig. 11. The motion is a pure single harmonic oscillation. Corresponding to the LCO motion, the oscillating frequency is shown in Fig. 10b. The frequency varies from 1.612 to 1.722 Hz for $u = 30.51$–35 m/s, which is between the plunge ($\omega_h = 1.5$ Hz) and pitch ($\omega_\phi = 2$ Hz) natural frequencies.

Figure 12 shows a limit cycle pitch amplitude (rms) vs flow velocity for an initial angle of $\theta_0 = 10$ deg. Compared to Fig. 10a, there is a rapid increase of the amplitude near the linear critical flutter velocity ($u_{cr} = 45$ m/s). When $u = 44.9$ m/s, the system is stable and tends to a static equilibrium position. When $u = 45$ m/s, the system tends to a LCO with a larger

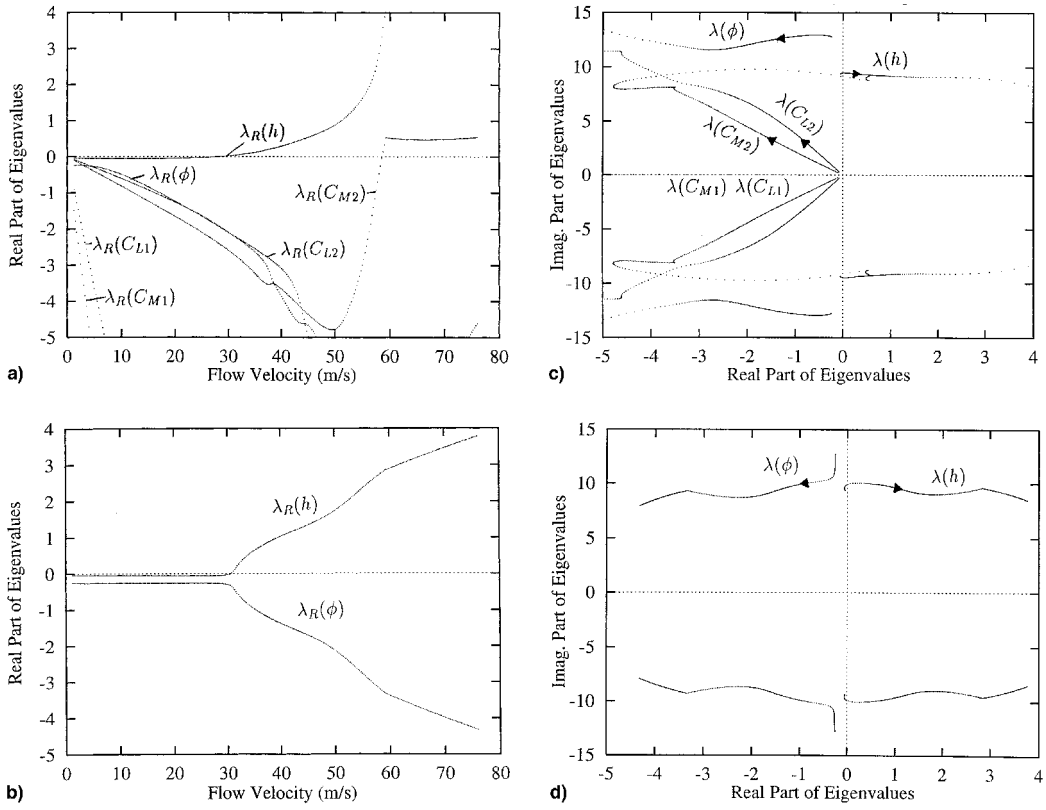

Fig. 8 Eigenvalue solutions of the linear model for $\theta_0 = -5$ deg, $x_m = -0.06$: a) real part, c) root-locus, the arrows indicates the direction of motion of the loci when u increases. b) and d) from the quasisteady aerodynamics.

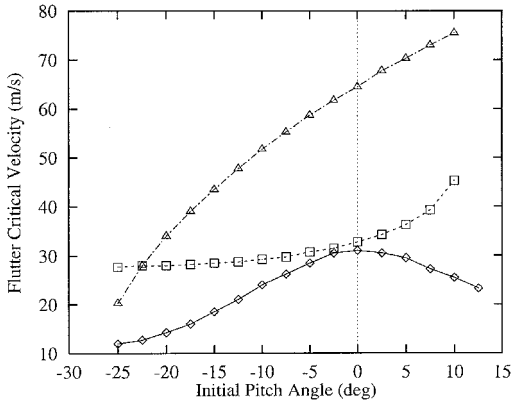

Fig. 9 Linear flutter solutions vs initial pitch angle for $x_{\alpha_h} = -0.06$, □, results from the quasisteady aerodynamics; and △ and ◇, from unsteady aerodynamics.

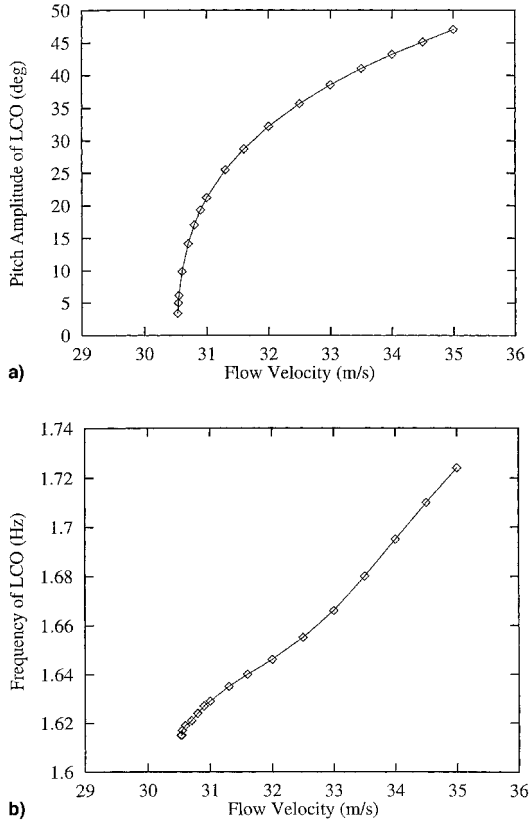

Fig. 10 Pitch LCO vs flow velocity for $\theta_0 = -5$ deg, $x_{\alpha_h} = -0.06$ using quasisteady aerodynamics: a) amplitude of LCO and b) frequency.

amplitude, as shown in Fig. 13a of the time history. The steady motion is almost periodic with a dominant frequency (1.66 Hz) and higher harmonic components (multiples of fundamental frequency). This behavior can be seen from the Poincare map for $\dot{h} \equiv 0$ (Fig. 13b). In Fig. 13b the map points are concentrated in two ranges. Because the Poincare section is taken when $\dot{h} \equiv 0$ (Fig. 13b), there are two points for one cycle in the map. When $u > 51$ m/s, the system is divergent.

Results for the unsteady case: With unsteady aerodynamics, the LCO behavior is not observed for all initial pitch angles as was seen for the quasisteady case. Now LCO is found only for the higher initial pitch angles ($\theta_0 > 8$ deg) and, otherwise, the motion is divergent when $u \geq u_{cr}$ or tends to a static equilibrium position when $u < u_{cr}$. Figure 14 shows a limit cycle pitch amplitude (rms) vs flow velocity for an initial angle of $\theta_0 = 10$ deg. It is very clear there is a jump in response at the

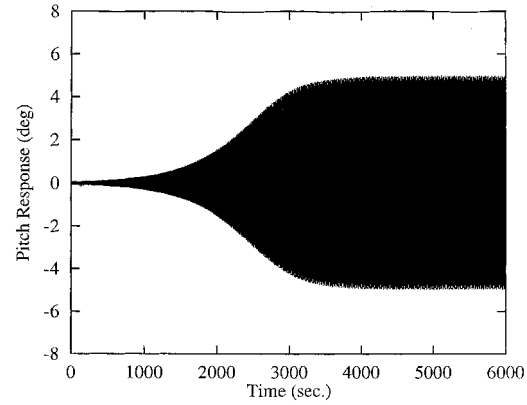

Fig. 11 Time history of the pitch response for $\theta_0 = -5$ deg, $u = 30.52$ m/s.

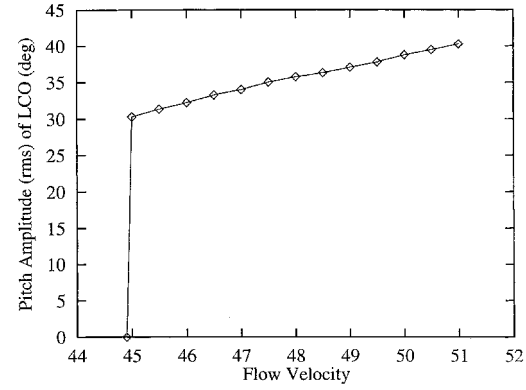

Fig. 12 Pitch amplitude (rms) of LCO vs flow velocity for $\theta_0 = 10$ deg, $x_{\alpha_h} = -0.06$ using quasisteady aerodynamics.

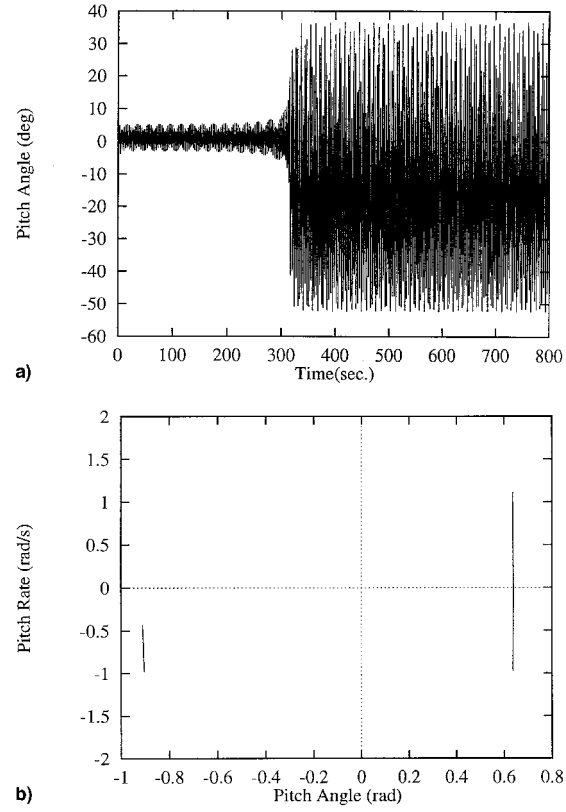

Fig. 13 Motion behavior of the pitch LCO for $\theta_0 = 10$ deg, $x_{\alpha_h} = -0.06$ using quasisteady aerodynamics: a) time history and b) Poincare map plot.

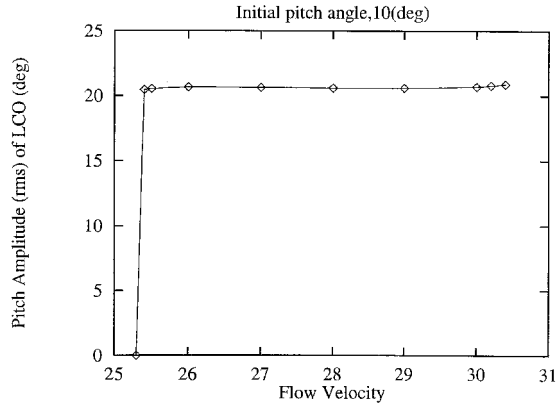

Fig. 14 Pitch amplitude (rms) of LCO vs flow velocity for θ_o = 10 deg, $x_{\alpha m}$ = −0.06 using unsteady aerodynamics.

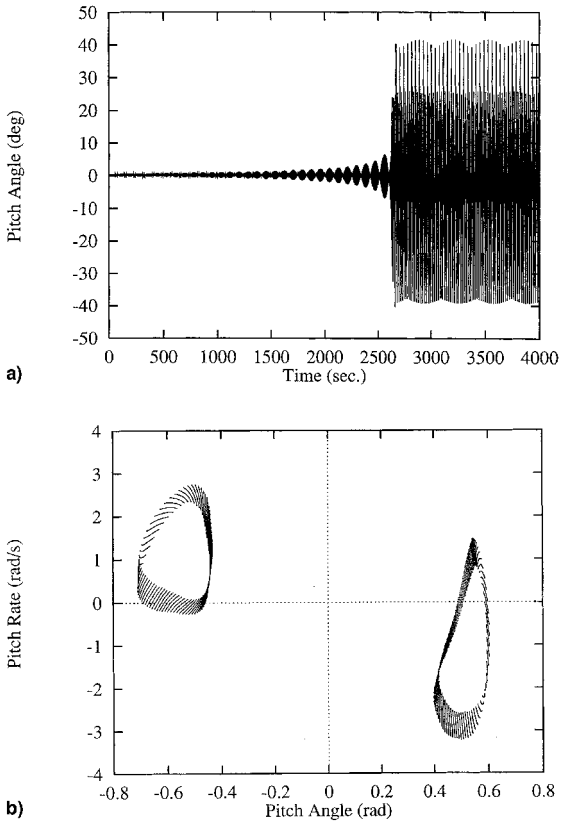

Fig. 15 Motion behavior of the pitch LCO for θ_o = 10 deg, $x_{\alpha m}$ = −0.06 using unsteady aerodynamics: a) time history and b) Poincare map plot.

linear critical flutter velocity (u_{cr} = 25.4 m/s). There is no LCO with a smaller amplitude and the LCO amplitude varies only slightly in the velocity range (25.4 m/s < u < 30.4 m/s). Compared to the quasisteady case for the same initial pitch angle, the flow velocity for the LCO response decreases from (45 to 25.4 m/s) and the steady LCO motion becomes more complex. The unsteady aerodynamics, particularly the stall equations, play an important role in the aeroelastic response. Figure 15a shows the time history of pitch motion for u = 25.4 m/s (minimum flow velocity for the onset of LCO). The transient process is quite long (about 2600 s) before the steady LCO motion is reached. The Poincare map for $\dot{h} \equiv 0$ is shown in Fig. 15b. Two frequency components are significant. One is associated with the structural motion (plunge) with a frequency of 1.63 Hz and another with the coupling between the aerodynamic pitch moment and structural pitch motion, 2.2 Hz. Because of the stronger second component and hysteresis aerodynamics,

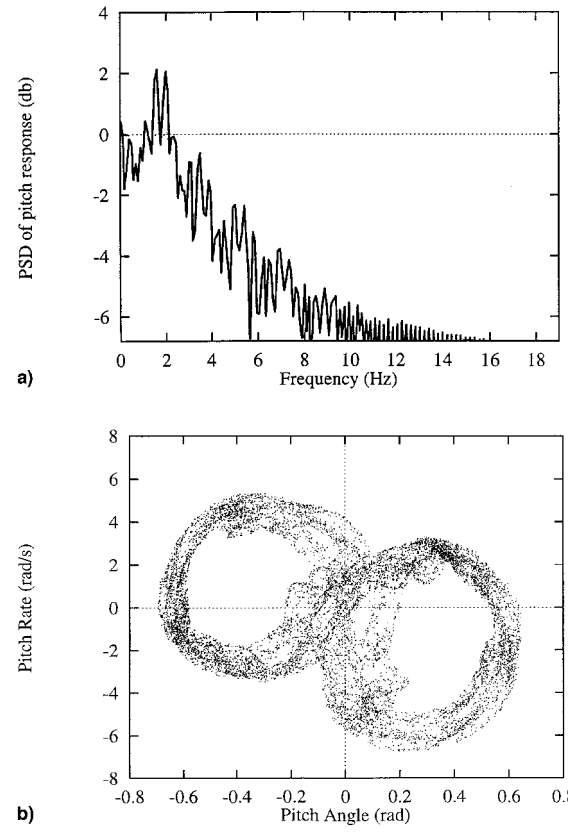

Fig. 16 Motion behavior of the pitch LCO for θ_o = 12.5 deg, $x_{\alpha m}$ = −0.06 using unsteady aerodynamics: a) power spectral density plot and b) Poincare map plot.

the Poincare map also becomes more complex. When the flow velocity increases beyond 25.4 m/s, the steady-state LCO motion changes only slightly but the transient process becomes shorter. For example, when u = 30 m/s, the transient is of about 50 s duration.

When we increase initial pitch angle further, say to θ_o = 12.5 deg, the coupling between the aerodynamic pitch moment and structural pitch motion becomes stronger as shown in the power spectral density plot (Fig. 16a). The magnitude of this component is almost equal to the first frequency component. The motion, now dominated by the nonlinear aerodynamics, becomes chaotic-like, as shown in Fig. 16b, the Poincare map.

VI. Concluding Remarks

This paper describes an innovative numerical procedure to determine quasisteady and unsteady aerodynamic coefficients of an external store of an aircraft. The experimentally identified unsteady aerodynamic model is then used to calculate the nonlinear aeroelastic response.

1) The new experimental method proposed by the present paper is an efficient and low-cost technique to identify the unsteady, separated-flow aerodynamic coefficients for a complex store structure of an aircraft. The results are verified by the good correlation between theoretical prediction and aerodynamic measurement.

2) Using the experimentally identified unsteady aerodynamic model to calculate the stability (flutter) and nonlinear aeroelastic response, it is shown that there is a large difference with the results obtained from the quasisteady aerodynamic model, particularly for the larger initial pitch angles. For an aircraft with an external store structure and at a high angle of attack, the unsteady aerodynamic model should be considered.

3) A smaller LCO amplitude is predicted to occur for the unsteady aerodynamic model than that for the quasisteady model beyond the linear flutter velocity. However, the limit

cycle amplitude predicted was so large that, because of safety concerns, no LCO experiments were done with the aeroelastic wind-tunnel model.

Acknowledgments

This work was supported under the U.S. Air Force Office of Scientific Research Grant, Limit Cycle Oscillations and Nonlinear Aeroelastic Wing Response. C. I. "Jim" Chang and Brian Sanders were the Grant Monitors.

References

[1]Dowell, E. H., and Ilgamov, M., *Studies in Nonlinear Aeroelasticity*, Springer–Verlag, New York, 1988.

[2]Dowell, E. H., Virgin, L. N., Tang, D. M., and Conner, M. D., "Nonlinear Dynamics of Aeroelastic Systems," *Proceedings of the CEAS Confederation of European Aerospace Societies, International Forum on Aeroelasticity and Structural Dynamics* (Rome, Italy), Vol. I, 1997, pp. 79–92.

[3]Liiva, J., Davenport, F. J., Grey, L., and Walton, I. C., "Two-Dimensional Tests of Airfoils Oscillating Near Stall," U.S. Army Aviation Material Lab., TR-68-13, Sept. 1968.

[4]Carta, F. O., "Analysis of Oscillatory Pressure Data Including Dynamic Stall Effects," NASA CR-2394, Feb. 1974.

[5]Carr, L. W., McAlister, K. W., and McCroskey, W. J., "Dynamic Stall Experiments on the NACA 0012 Airfoil," NASA TP-1100, Jan. 1978.

[6]Hilaire, A. O., and Carta, F. O., "Analysis of Unswept and Swept Wing Chordwise Pressure Data from an Oscillating NACA 0012 Airfoil Experiment," Vol. 1, Tech. Rept., NASA CR 3567, March 1983.

[7]Hilaire, A. O., and Carta, F. O., "Analysis of Unswept and Swept Wing Chordwise Pressure Data from an Oscillating NACA 0012 Airfoil Experiment," Vol. 2, Data Rept., NASA CR 165927, June 1983.

[8]McCroskey, W. J., McAlister, K. W., Carr, L. W., and Pucci, S. L., "An Experimental Study of Dynamic Stall on Advanced Airfoil Sections, Volume 1, Summary of the Experiment," NASA TM 84245, July 1982.

[9]Reddy, T. S. R., and Kaza, K. R. V., "A Comparative Study of Some Dynamic Stall Models," NASA TM 88917, March 1987.

[10]Piziali, R. A., "2-D and 3-D Oscillating Wing Aerodynamics for a Range of Angles of Attack Including Stall," NASA TM 4632, Sept. 1994.

[11]Petot, D., "Differential Equation Modeling of Dynamic Stall," *La Recherche Aerospatials*, Vol. 5, No. 5, 1989, pp. 59–72.

[12]Favier, D., Agnes, A., Barbi, C., and Maresca, C., "Combined Translation/Pitch Motion: A New Airfoil Dynamic Stall Simulation," *Journal of Aircraft*, Vol. 25, No. 9, 1988, pp. 805–814.

[13]Tang, D. M., and Dowell, E. H., "An Experimental Investigation of a Three-Dimensional Dynamic Stall Model Oscillating in Pitch," *Journal of Aircraft*, Vol. 32, No. 5, 1995, pp. 1062–1071.

[14]Tang, D. M., Paul, G. A. Cizmas, and Dowell, E. H., "Experiments and Analysis for a Gust Generator in a Wind Tunnel," *Journal of Aircraft*, Vol. 33, No. 1, 1996, pp. 139–148.

[15]Ozcan, O., Unal, M. F., Aslan, A. R., Bozkurt, Y., and Aydin, N. H., "Aerodynamic Characteristics of External Store Configuration at Low Speeds," *Journal of Aircraft*, Vol. 32, No. 1, 1995, pp. 161–170.

[16]Tobak, M., "On the Minimization of Airplane Responses to Random Gusts," NACA TN 3290, May 1957.